Check for updates

ADVANCED MATERIALS TECHNOLOGIES
www.advmattechnol.de

3D-Printed Mixed Ionic-Electronic Conductive Polymer Composites for Long-Term Bioelectronic Sensing

*Simone Bagatella, Heejung Roh, Marco Cavallaro, Raffaella Suriano, Marinella Levi, and Aristide Gumyusenge**

Reliable, long-term monitoring of health data is becoming increasingly essential in modern healthcare. While computational and machine learning capabilities continue to advance, the lack of lightweight, conformable, and customizable hardware remains a key limitation. In the context of heart health, traditional electrocardiogram (ECG) electrodes are rigid and often uncomfortable for continuous wear. Existing soft electrodes tend to be either cost-prohibitive or unreliable over extended use. In this work, all-polymer, 3D-printed, highly stable, and conformable ECG patches are developed for long-term signal acquisition. Through material optimization, composite materials with electrical conductivity up to 1.7 S cm^{-1} are developed, maintaining over 85% of their conductivity after 60 days of exposure to open air. These materials also exhibit remarkable stretchability (strain at break up to 253%) and high mechanical strength (tensile strength of 25 MPa). The formulated inks are fully compatible with 3D material extrusion techniques, significantly reducing manufacturing costs. The printed electrodes are flexible, stretchable, and capable of recording high-quality ECG signals, performing comparably to state-of-the-art metal electrodes, even after more than a month of use-and-store in open air.

1. Introduction

Medical devices that can autonomously and continuously monitor physiological signals, while simultaneously enabling data-driven therapeutic intervention, hold the potential to revolutionize modern healthcare and dramatically reduce morbidity and mortality.[1–4] A notable example is the increasing prevalence of wearable technologies in diabetes management.[5–10] Continuous glucose monitors (CGMs), when integrated with insulin pumps, enable closed-loop glycemic control, minimizing human error and removing the guesswork associated with manual insulin dosing.[11,12] These closed-loop systems significantly improve clinical outcomes and patient quality of life. However, such integrated sensing-feedback architectures are still rare for other major diseases. Conditions such as cardiovascular disorders, cancer, and mental health illnesses—which collectively account for over 647 000 deaths, 600 000 deaths, and 47 million severe cases annually in the United States alone (as of 2021)[6]—stand to benefit immensely from real-time physiological monitoring coupled with automated or semi-automated treatment systems. By reducing dependence on frequent clinical visits, enabling earlier intervention, and lowering diagnostic error, such systems can alleviate strain on healthcare infrastructures, reduce treatment costs, and expand access to underserved populations.

Enabling this vision requires robust, reliable, and biocompatible electronic interfaces that can maintain long-term performance on or in the human body. In this context, polymer-based electronics are gaining increasing interest due to their mechanical softness, chemical tunability, and intrinsic compatibility with biological tissues.[8,13–17] Unlike traditional rigid materials, conductive and semiconductive polymers can be engineered to match the mechanical properties of skin, muscles, and organs, thereby minimizing discomfort, reducing motion artifacts, and ensuring long-term adhesion.[14] However, despite their promise, many polymeric systems continue to face key limitations in signal stability, environmental durability, and scalable manufacturability.

For electrophysiological applications such as electrocardiography (ECG), where high signal fidelity and uninterrupted skin contact are critical, these limitations must be addressed before polymer-based medical devices can become ubiquitous.[18–20] Conventional ECG electrodes, typically composed of rigid metals or gel-based conductors, are poorly suited for prolonged use due to issues such as discomfort, skin irritation, and degradation

S. Bagatella, H. Roh, A. Gumyusenge
Department of Materials Science and Engineering
Massachusetts Institute of Technology
Cambridge, MA 02139, USA
E-mail: aristide@mit.edu
S. Bagatella, M. Cavallaro, R. Suriano, M. Levi
Department of Chemistry
Materials and Chemical Engineering "Giulio Natta", Politecnico di Milano
Milano 20133, Italy

The ORCID identification number(s) for the author(s) of this article can be found under https://doi.org/10.1002/admt.202501154

© 2025 The Author(s). Advanced Materials Technologies published by Wiley-VCH GmbH. This is an open access article under the terms of the Creative Commons Attribution License, which permits use, distribution and reproduction in any medium, provided the original work is properly cited.

DOI: 10.1002/admt.202501154

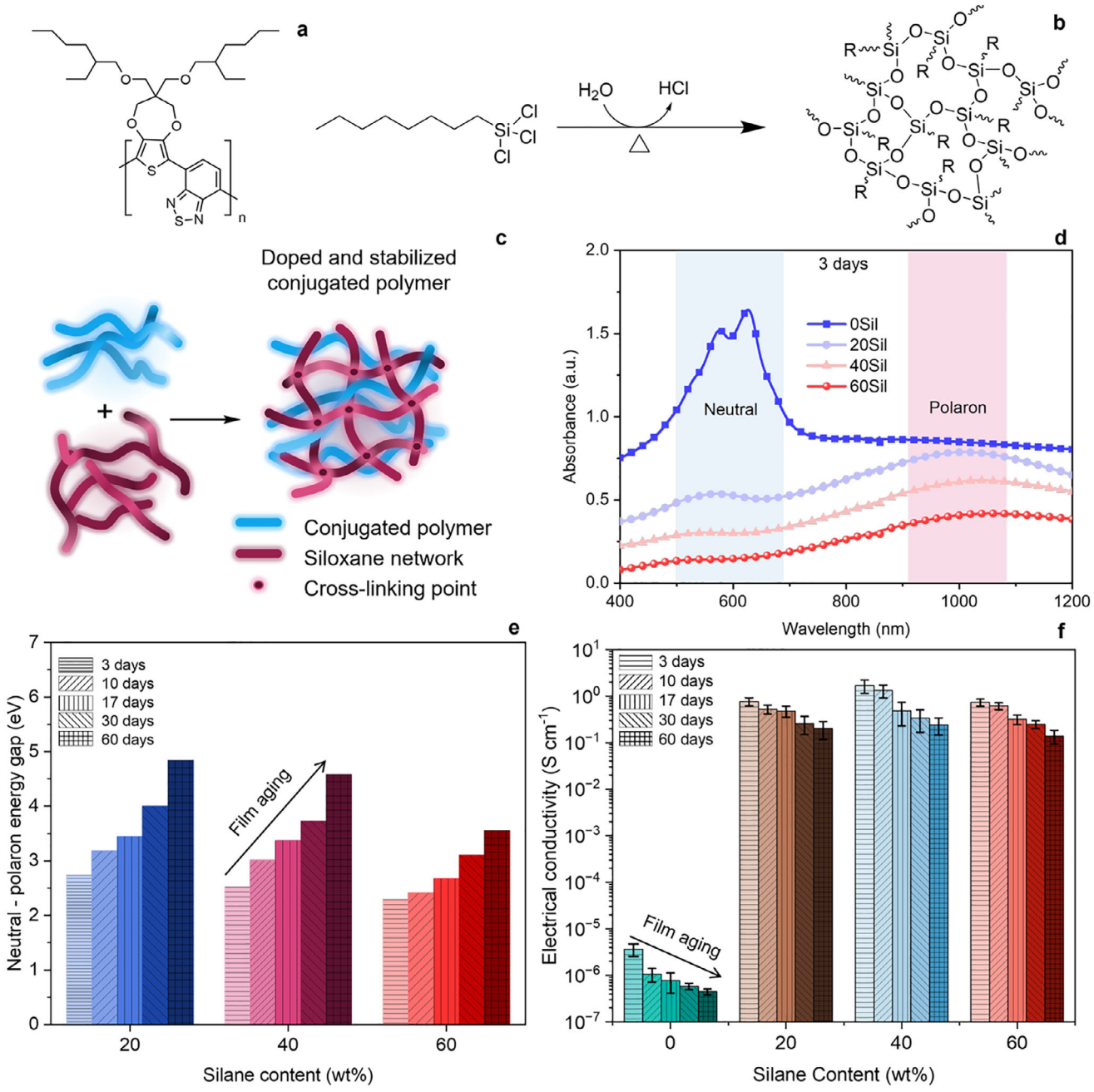

Figure 1. Design of a siloxane-based composite: a) chemical structure of the conjugated polymer; b) thermal condensation of chlorosilane forming a crosslinked siloxane network (R denotes the octyl chain); c) illustration of a CP-siloxane composite. Characterization of the doping effects as a function of chlorosilane content: d) UV–vis absorption spectra after 3 days; e) energy difference between neutral and polaronic absorption peaks and f) electrical conductivity evolution over time (3, 10, 17, 30, and 60 days). The error bars represent the standard deviation from three representative samples for each formulation ratio monitored for 2 months.

over time.[21–23] Although alternative soft electrode platforms—including hydrogel, textile, and elastomer-based patches—have been developed, these systems often struggle with fabrication complexity, high costs, and limited long-term operational stability.[8,17,24–26] In that regard, additive manufacturing (AM) techniques, especially material extrusion 3D printing, offer a scalable, cost-effective, and sustainable route for fabricating body-conformable electronics, especially on-body electrodes.[27,28] This approach enables rapid prototyping, digital design flexibility, and direct integration of functional materials onto a variety of substrates.

Though several examples have been successful as summarized in a recent review by Zhang et al.,[29] realizing printable, long-lasting, and high-performing polymeric electrodes (e.g., ECG electrodes) remains a key materials challenge.[30–34] To date, most polymer-based conductive systems rely on polymer doping and

© 2025 The Author(s). Advanced Materials Technologies published by Wiley-VCH GmbH

2365709x, 2025, 24, Downloaded from https://advanced.onlinelibrary.wiley.com/doi/10.1002/admt.202501154 by POLITECNICO DI MILANO, Wiley Online Library on [20/03/2026]. See the Terms and Conditions (https://onlinelibrary.wiley.com/terms-and-conditions) on Wiley Online Library for rules of use; OA articles are governed by the applicable Creative Commons License

often exhibit reduced conductivity after repeated use or exposure to ambient environments, limiting their long-term utility in real-world settings.[17] Many designs (for instance PEDOT:PSS-based materials) rely on multiple additives and/or encapsulation strategies to maintain performance in ambient conditions,[35,36] which complicates their extrudability. Such stability challenges commonly arise from the inability of doped polymers to maintain that state for extended periods of time, especially under dynamic environments.[37,38] Having access to simplified ink formulations that yield high-performing and reliable electrodes would propel the widespread use of extrusion methods such as 3D printing of polymer electronics.

In this work, we report a fully 3D-printable, all-polymer ECG monitoring platform that overcomes the limitations of current technologies particularly in terms of signal quality and long-term stability. Our approach uses a conductive composite based on an organic mixed ionic-electronic conductor (OMIEC) and a siloxane crosslinked network. By systematically tuning the formulation of the conductive composite, we establish key structure–property relationships that enable environmental stability, mechanical compliance, and electrical performance. Notably, the incorporation of siloxane not only improves the composite's environmental durability but also enhances its electrical conductivity, reaching values as high as 1.7 S cm^{-1}. This level of conductivity was preserved after over 1 month of open-air storage, without the need for encapsulation or additional protection. Furthermore, we demonstrate that these composites are compatible with common 3D printing techniques. The inks exhibit excellent rheological properties, achieving a printability index of 1.01, indicating optimal flow behavior for high-resolution patterning. Without any additional formulation steps, the materials can be printed into uniform films with consistent thickness and mechanical integrity. We leveraged this capability to fabricate stretchable, conformal ECG electrodes, which successfully recorded high-fidelity heart signals continuously for over 40 days without signs of mechanical or electrical failure. Our results establish a new pathway for developing scalable, long-lasting, and cost-effective wearable electronics.

2. Results and Discussion

2.1. Effects of Siloxane Network Formation on the Conjugated Polymer

Deploying the unique applicability of organic mixed ionic-electronic conductors (OMIECs) often requires addressing key challenges such as mechanical stretchability, electrical conductivity, and long-term stability.[39–42] OMIECs, despite their promising and unique properties, tend to suffer from modest stability as well as electrical conductivity. In the context of these challenges, we turned to the formulation of a composite that combines a mixed-ionic electronic conductor with a silane-based crosslinker (**Figure 1a–c**).[43–46] More details on the formulation, processing, and physical characterization of the composites can be found in the experimental section and the Supporting Information. Inspired by our previous works on the processability and silane-doping of conjugated polymers,[43,44] in this work, we selected 3,4-propylenedioxythiophene 2,1,3-benzothiadiazole (ProDOT-BT) as the conjugated polymer (CP) and trichloro(octyl)silane (Sil) (Figure 1a,b) to form conductive composites (Figure 1c; Figure S1, Supporting Information). ProDOT-BT offers both facile solution-processability and a semicrystalline morphology, enabling the formation of an interpenetrating network between its chains and the siloxane network.[44,46] Upon crosslinking, Sil forms a siloxane network through one reactive end, leaving the octyl group free to co-crystallize with CP crystallites. We hypothesized that employing a single-sided silane would enable moderate crosslinking,[44] thus allowing effective doping and stabilization without further disrupting the inherent crystallization of CP (Figure 1c). The incorporation of the siloxane crosslinker serves multiple purposes: 1) it establishes a mechanically robust, elastomeric network that imparts stretchability and conformability to the composite films, and 2) it enhances resistance to moisture and oxidative agents. Moreover, this structural modification has been shown to substantially increase the electrical conductivity of conjugated polymers through acid doping, the byproduct of the crosslinking reaction. Conductivity values as high as 1.0 S cm^{-1}, a range that is inherently challenging to attain in comparable polymer systems, especially systems using one additive or dopant, were achieved xSil composites.[44,47,48]

2.2. Stable Doping of Conjugated Polymer

To investigate the doping efficiency in the composite system and monitor its long-term stability, UV–vis spectroscopy was performed over time. As shown in Figure 1d and Figure S2 (Supporting Information), the absorption spectrum of the pristine CP film (0Sil) shows the characteristic vibronic peaks at 575 and 626 nm, corresponding to its neutral state, with an optical bandgap of ≈1.8 eV. Upon crosslinking with chlorosilane, a broad absorption at ≈1000 nm was observed, indicative of polaron formation and consistent with the doping of the CP during the crosslinking reaction. Increasing the chlorosilane content (up to 60 wt.% in this case) led to a progressive increase in the polaron peak suggesting a more favorable doping state. Despite a gradual decrease in intensity overtime, this polaron absorption band persisted over time, monitored up to 60 days (Figure 1e; Figure S2, Supporting Information), suggesting long-term stability of the conductive composites. Though the silane-based doping of CP has been studied before,[44,46] this retention of the doped state has rarely been characterized.

The electrical conductivity measurements revealed a significant enhancement in electrical properties upon chlorosilane incorporation, with an increase of up to six orders of magnitude compared to the undoped CP, as shown in Figure 1f. Specifically, the conductivity of the pristine CP, which exhibited semiconducting behavior with an electrical conductivity of $3.6 \cdot 10^{-6}$ S cm^{-1}, increased to 0.77, 1.7, and 0.70 S cm^{-1} for chlorosilane contents of 20, 40, and 60 wt.%, respectively. The maximum conductivity was observed at 40 wt.%, suggesting that at higher chlorosilane concentrations, there is a likelihood of forming isolated siloxane domains which may hinder charge transport. This enhancement was in agreement with previous reports utilizing the HCl crosslinking by-product to dope conjugated polymers.[46] Note that increasing the Sil content in the composites also impacts other properties such as charge capacity and electrochemical impedance, as shown in Figures S3 and S4 (Supporting

© 2025 The Author(s). Advanced Materials Technologies published by Wiley-VCH GmbH

2365709x, 2025, 24, Downloaded from https://advanced.onlinelibrary.wiley.com/doi/10.1002/admt.202501154 by POLITECNICO DI MILANO, Wiley Online Library on [20/03/2026]. See the Terms and Conditions (https://onlinelibrary.wiley.com/terms-and-conditions) on Wiley Online Library for rules of use; OA articles are governed by the applicable Creative Commons License

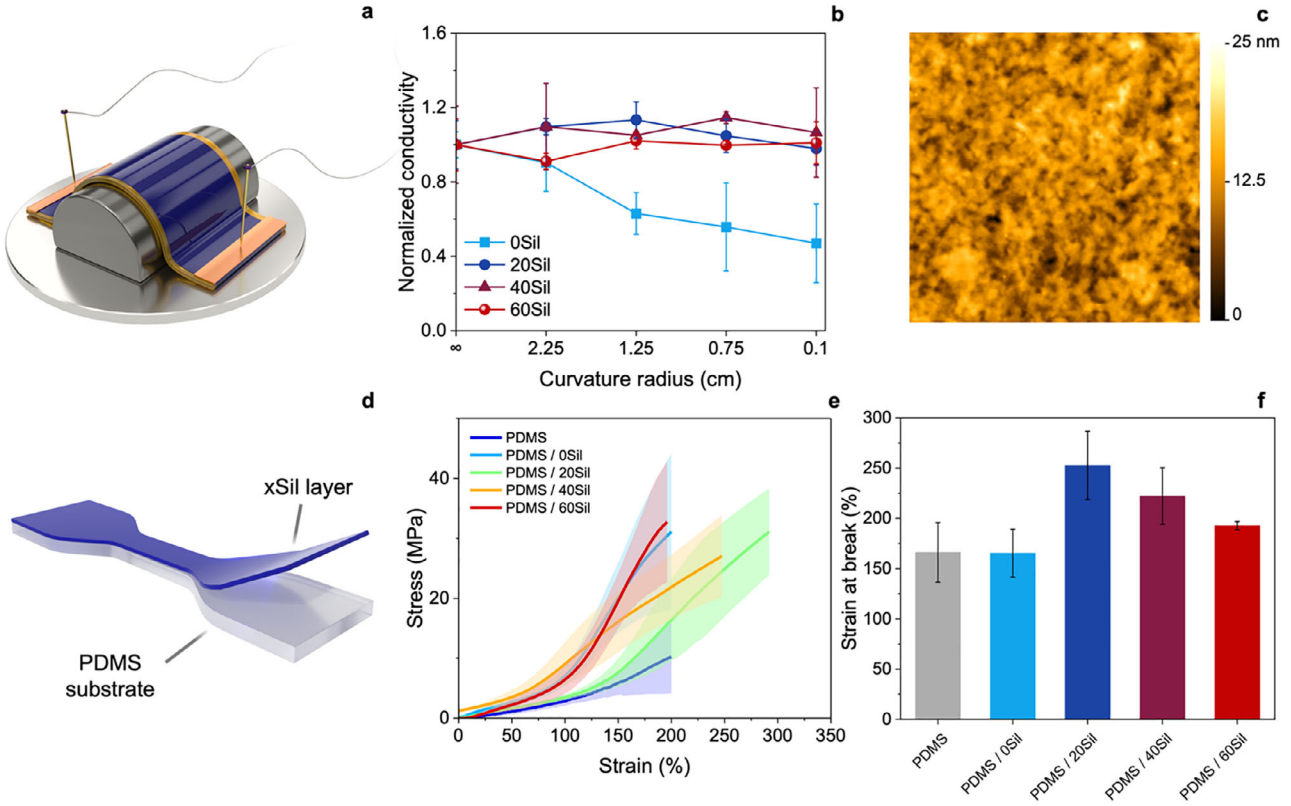

Figure 2. a) Scheme of the polymer composite coated onto a flexible Kapton substrate for electrical conductivity measurements upon bending; b) normalized conductivity of the polymer films with different chlorosilane contents as a function of the curvature radius. t; c) AFM image of 20Sil; d) scheme of a double-layered structure consisting of a PDMS substrate and a polymer layer for dog-bone tensile test specimens; e) stress-strain curves of the composite structure with polymer films with different chlorosilane contents (the shading represent standard deviations from three different specimens measured for each ratio); f) strain at break of the composites at different chlorosilane contents.

Information), indicating that careful balance between the crosslinking density and electrode performance must be considered depending on the intended use case.

Besides the improvement in conductivity, the stability of the doped system over time was assessed for up to 60 days following material processing. The electrical conductivity remained stable over this period, with only a minor decrease of one order of magnitude after 60 days when the films were left exposed to ambient conditions. This stability indicates a sustained doping effect, likely due to the entrapment of doping species within the siloxane matrix. Note that upon crosslinking, a uniform and homogenous morphology is formed, indicating that a well-interpenetrating network between CP and Sil is formed (Figure S5, Supporting Information). The crosslinked structure may act as a protective environment, preventing dopant diffusion and mitigating oxidative degradation under ambient conditions. This retention of electrical conductivity in doped polymer films is commonly challenging to achieve in polymer systems, particularly in single-dopant approaches.[37,38]

2.3. Mechanical Properties of the Crosslinked Composites

Besides stable conductivity, bioelectronics and wearable technologies also necessitate materials that exhibit minimal degradation when subjected to mechanical stress.[13] We thus evaluated the stabilizing effect of siloxane crosslinking on the mechanical flexibility and stretchability of the composites. First, electrical conductivity measurements were performed under different bending conditions three days after fabrication. The polymer films were coated onto a flexible Kapton substrate, and their resistance was monitored as a function of curvature radius, ranging from a flat configuration (infinite curvature radius) to progressively higher bending deformations (**Figure** 2a; Figure S6, Supporting Information). As shown in Figure 2b, the pristine CP films (0Sil) exhibited a significant decrease in electrical conductivity under mechanical deformation. Upon bending, the normalized conductivity dropped to 47 (±21) % of its initial value in the flat configuration (Figure 2b), suggesting that mechanical strain disrupts the percolation pathways of charge carriers in the pristine CP film, leading to a substantial loss in electrical performance.

In contrast, incorporating chlorosilane crosslinkers demonstrated to enhance stable conductivity under the same bending conditions. Regardless of the curvature radius, the normalized conductivity remained within the standard deviation, with variations generally limited to ± 15% of the initial value (Figure 2b). This stability suggests that the siloxane network acts as a structural reinforcement, mitigating mechanical strain effects and preventing significant morphological disruptions within the CP

© 2025 The Author(s). Advanced Materials Technologies published by Wiley-VCH GmbH

2365709x, 2025, 24, Downloaded from https://advanced.onlinelibrary.wiley.com/doi/10.1002/admt.202501154 by POLITECNICO DI MILANO, Wiley Online Library on [20/03/2026]. See the Terms and Conditions (https://onlinelibrary.wiley.com/terms-and-conditions) on Wiley Online Library for rules of use; OA articles are governed by the applicable Creative Commons License

bulk. The ability to maintain consistent electrical properties under deformation highlights the potential of these materials for use in soft and wearable electronics, where mechanical flexibility is a critical requirement for practical implementation. Unlike rigid electronic materials, which can limit user comfort and adaptability in wearable applications, these polymer-siloxane composites provide an attractive alternative by offering both high electrical conductivity and stability under mechanical stress.

In terms of stretchability, CPs are typically prone to mechanical failure under strain, limiting their direct use in highly deformable systems.[49,50] We tested the silane-based composites on top of polydimethylsiloxane (PDMS) substrates (Figure 2d) and monitored the maximum stress supported as well as the strain at break. This configuration leverages the mechanical compliance of PDMS to enhance the overall flexibility and durability of the composite while maintaining the electrical functionality of the CP layer. The mechanical properties of the composite structures were evaluated through uniaxial tensile tests using dog-bone specimens (Figure S7, Supporting Information). Figure 2e shows the stress-strain curves of the samples with varying siloxane content. The control PDMS substrate exhibited mechanical behavior consistent with literature reports,[51] with a failure at a stress of 9.2 MPa and a strain at break of 166%. These values confirm the reproducibility of the PDMS mechanical response and its suitability as a compliant support layer. Upon incorporating the CP layer, a noticeable increase in stress-at-break was observed, indicating reinforcement of the composite system. Specifically, the addition of pristine CP (0Sil) led to increased stress-at-break up to 25.4 MPa, whereas the strain at break remained comparable to that of the pristine PDMS, suggesting that while the CP layer contributed to mechanical reinforcement, it did not significantly alter the stretchability of the system.

A significant enhancement in mechanical stretchability was observed when the CP was processed with a siloxane network. While the stress at break remained relatively unchanged, the strain at break exhibited a progressive increase as the siloxane content increased. Notably, the 20 wt.% siloxane composite (20Sil) demonstrated the highest stretchability, with the strain at break improving from 165% in the pristine CP composite to 253%. This behavior suggests that the siloxane network not only facilitates stress distribution within the composite but also improves interfacial adhesion between the CP layer and the PDMS substrate. The chemical interactions between the siloxane-functionalized CP and the PDMS matrix likely contribute to enhanced load transfer, thereby allowing the composite to sustain higher deformation before failure. At higher siloxane contents (40Sil and 60Sil), a gradual decrease in strain at break was observed. This reduction may be attributed to the morphological structure, which can lead to embrittlement and reduced elongation capacity. However, despite this decrease, all siloxane-modified composites exhibited higher stretchability compared to the pristine CP, indicating that the siloxane network plays a key role in improving the mechanical resistance of the system. Beyond tensile strength and elongation, the toughness of the composites was also evaluated by calculating the energy under the stress-strain curve, a critical factor for applications requiring durable and deformable electronic materials. The toughness increased from 2250 MPa of Sil0, to 3231, 3153, and 2083 MPa, for 20Sil, 40Sil, and 60Sil, respectively, suggesting that the incorporation of siloxane enhances the mechanical toughness of the composites, further supporting their suitability for flexible electronic applications.

2.4. Formulation of Conductive Inks for 3D printing Flexible Electrodes

One of the key advantages of CPs lies in their inherent processability of polymer materials and their tunable properties, distinguishing them from conventional semiconductors that require high-temperature processing, leading to increased energy consumption and less sustainable manufacturing routes. While CPs are commonly processed via solution-based techniques such as spin-coating or drop-casting, their integration with advanced fabrication methods remains a crucial step toward scalable and sustainable device manufacturing. In particular, additive manufacturing (AM) technologies offer an opportunity to fabricate complex architectures in a cost-effective and material-efficient manner, eliminating the need for masks, reducing waste, and enabling custom-designed structures. This aspect is particularly beneficial for bioelectronic applications, where tailored device geometries can enhance compatibility with the surrounding environment, integration with complex systems and ad hoc optimized performance.

To explore the feasibility of employing CP-based inks in extrusion-based 3D printing, the composite containing 20 wt.% of chlorosilane (20Sil) due to its balance of electrochemical and mechanical properties, was selected and formulated into printable inks. The 20Sil was dissolved in chloroform at a concentration of 20 wt.% to achieve the desired rheological characteristics for direct-ink writing (DIW). The ink exhibited pseudoplastic behavior (**Figure 3a**), which is crucial for smooth extrusion during the printing process. Additionally, amplitude sweep oscillatory tests (Figure 3b) showed a clear crossover point, corresponding to an average yield stress ≈222 Pa and a storage modulus (G′) to the order of 10^4 Pa. These values indicate that the ink is suitable for printing complex patterns, as it maintains structural integrity and prevents deformation or collapse post-printing.[52]

The printability of the ink was further examined in terms of shape fidelity, which is a critical factor in AM for producing well-defined features. The pore geometry test (Figure 3c,d) was conducted using square pore structures with characteristic dimensions ranging from 750 to 1500 µm to evaluate the ink's ability to maintain sharp edges and minimize deviations from the intended geometry. The printability index (P_r) was used as a metric to quantify shape fidelity, with values closer to 1 indicating highly accurate printing. As the pore dimension increased from 750 to 1000 µm and 1500 µm, the P_r decreased from 1.50 to 1.25 and ultimately to 1.01, demonstrating a progressive improvement in feature resolution. These results confirmed that the 20Sil-based ink can achieve high shape fidelity, particularly for structures with dimensions at least 7.5 times larger than the nozzle diameter.

Furthermore, filament fusion tests (Figure 3e,f) were performed to evaluate the ink's ability to produce well-defined features without unintended filament merging due to capillary-driven effects. The meandering filament test revealed an exponential decrease in the fused segment length (f_s) normalized by the filament width (f_w), consistent with previous studies.[53]

© 2025 The Author(s). Advanced Materials Technologies published by Wiley-VCH GmbH

2365709x, 2025, 24, Downloaded from https://advanced.onlinelibrary.wiley.com/doi/10.1002/admt.202501154 by POLITECNICO DI MILANO, Wiley Online Library on [20/03/2026]. See the Terms and Conditions (https://onlinelibrary.wiley.com/terms-and-conditions) on Wiley Online Library for rules of use; OA articles are governed by the applicable Creative Commons License

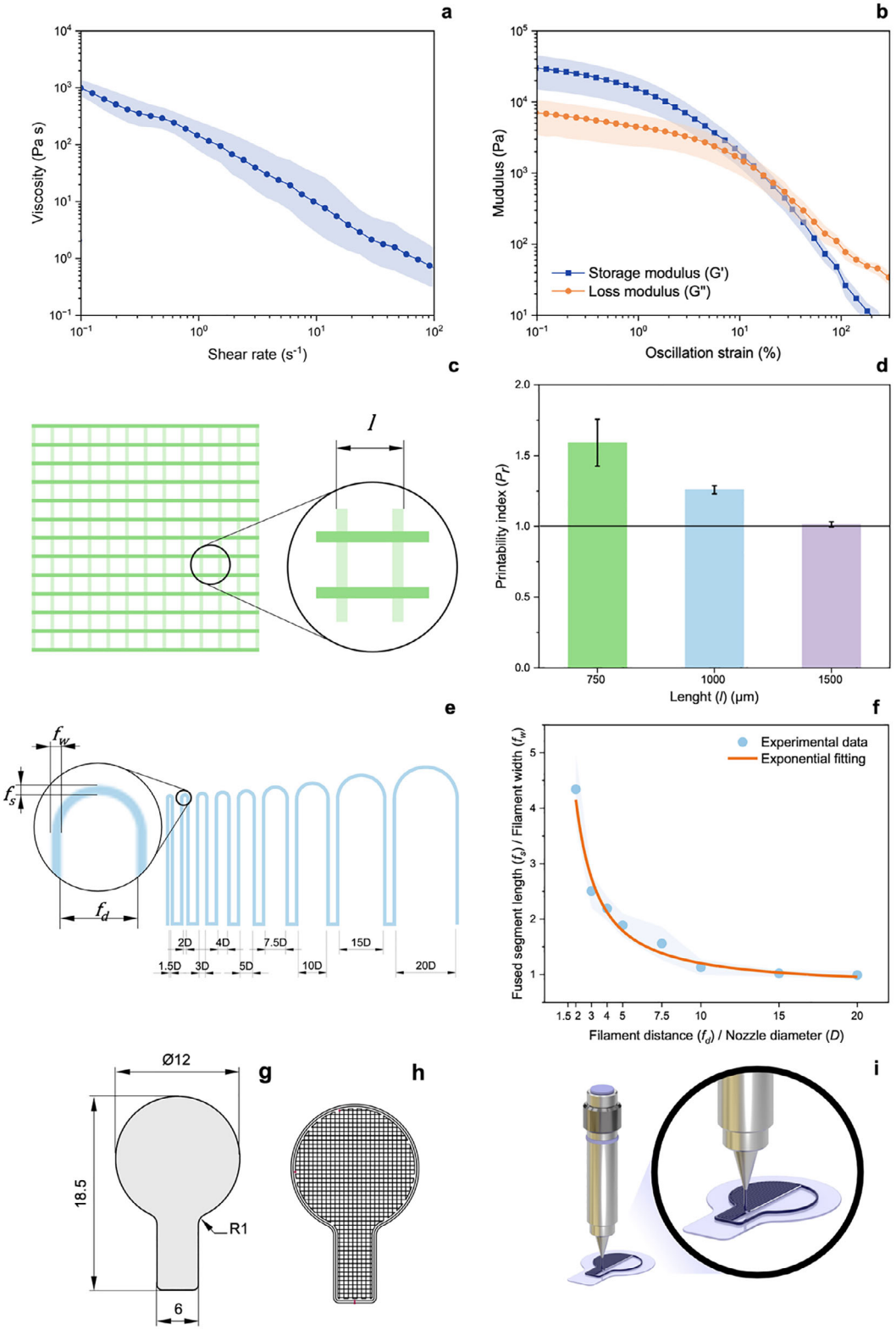

Figure 3. 3D printability assessment of the 20Sil-based ink via rheological and shape fidelity characterization: a) flow curve b) amplitude-sweep oscillatory test. Shape fidelity evaluation through c,d) pore structure test with varying pore sizes and e,f) filament fusion test. The shading represents the standard deviations from three 20Sil samples. 3D printing process of ECG patch: (g) design of the conductive layer of the patch, h) corresponding toolpath, and i) deposition of the 20Sil-based layer on PDMS.

© 2025 The Author(s). Advanced Materials Technologies published by Wiley-VCH GmbH

2365709x, 2025, 24, Downloaded from https://advanced.onlinelibrary.wiley.com/doi/10.1002/admt.202501154 by POLITECNICO DI MILANO, Wiley Online Library on [20/03/2026]. See the Terms and Conditions (https://onlinelibrary.wiley.com/terms-and-conditions) on Wiley Online Library for rules of use; OA articles are governed by the applicable Creative Commons License

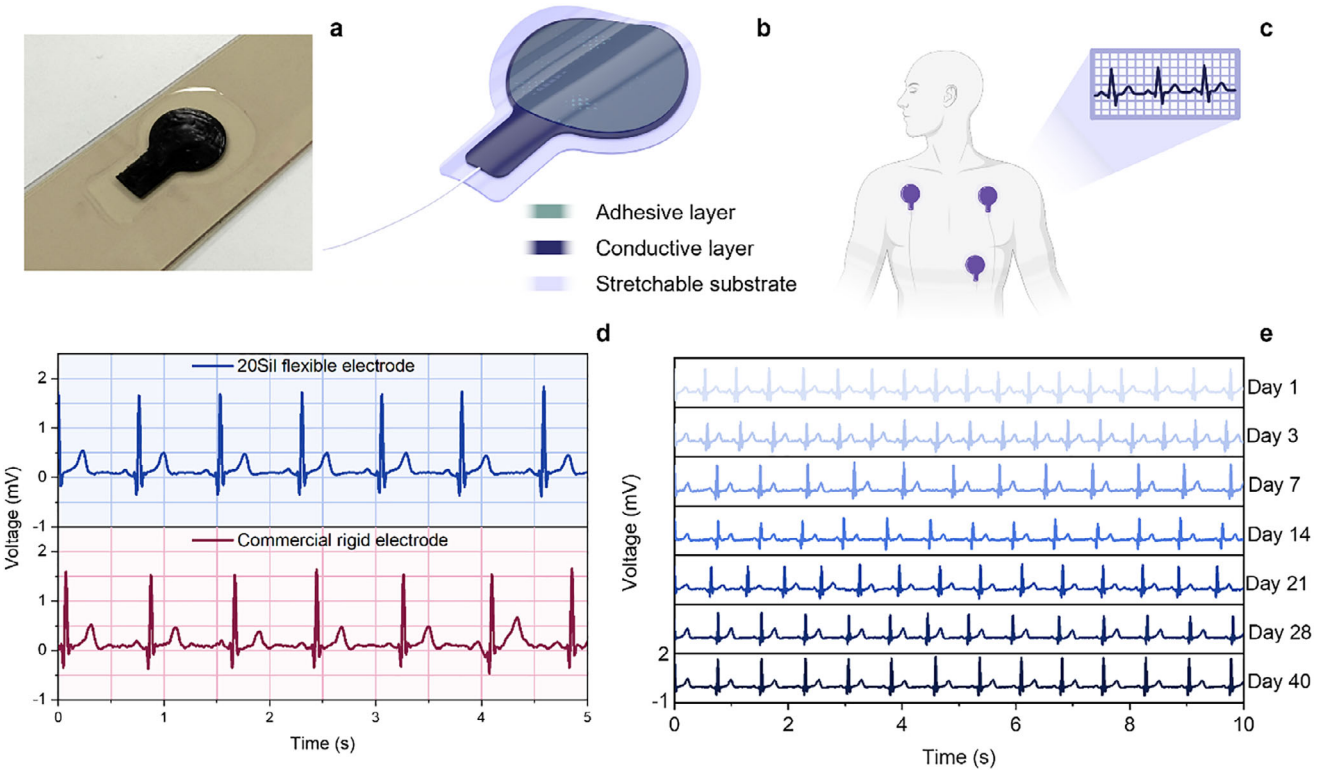

Figure 4. a) 3D-printed ECG patch via direct ink writing b) schematic illustration of flexible ECG patch structure for bioelectronic sensing, and c) ECG monitoring setup. Electrocardiogram signal measured with the 3D-printed flexible patch: d) comparison of ECGs recorded using a commercial rigid electrode and the fabricated flexible electrode based on 20Sil, and e) signal stability over time for up to 40 days.

The ideal condition of $f_s/f_w \approx 1$, where filaments maintain their intended width without merging, was achieved when the filament spacing was at least ten times the nozzle diameter. Notably, even at a spacing of five times the nozzle diameter, good printability was observed with f_s/f_w <2, demonstrating a balance between resolution and structural integrity. Overall, the optimized 20Sil-based ink demonstrated excellent rheological properties, enabling high-resolution patterning with reliable printability and shape fidelity.

Leveraging these characteristics, a flexible and conformal skin-interfacing patch was designed and fabricated via a two-step DIW process, integrating a bilayer structure to ensure both mechanical robustness and electrical functionality. The bottom insulating layer, made of PDMS, was 3D-printed after parameter optimization (Figure S8, Supporting Information). This layer served as an insulating support with mechanical robustness, as pointed out in the mechanical tests. On top of this insulating base, the optimized 20Sil-based conductive ink was printed following a predefined toolpath (Figure 3g,h), forming a flexible and stable electrode layer. To ensure biocompatibility and prolonged skin adherence, a commercial and biocompatible adhesive layer was applied (see Experimental details and Figure S9, Supporting Information). Note that though this adhesive layer was used as a precaution since cytotoxicity studies were beyond the scope of this work, we anticipate that the patches based on CP/Sil composites are bio-safe, in accordance with previous works on doped and crosslinked polymer films using similar chemical formulations.[36,54–57]

2.5. Stable and Flexible Patch Fabrication for Electrophysiological Sensing

Following the successful development and printing by DIW of flexible patches, the proof-of-concept device (**Figure** 4a,b) was tested to demonstrate its applicability in electronic applications. The patch was tested in a real-world electrophysiological monitoring scenario on human volunteers, specifically for ECG signal acquisition. The device was coupled with an external ECG monitoring system in a three-electrode configuration. This setup allowed for direct comparison with conventional rigid commercial electrodes (Figure 4d), evaluating the signal quality and stability over extended durations. The recorded ECG data exhibited signal amplitudes ranging from 1.7 to 2.0 mV, comparable to those obtained using standard rigid electrodes (Figure 4d; Figure S9, Supporting Information). The high signal fidelity enabled clear identification of essential ECG features, including the R-R interval and QRS complex, both of which are critical for medical diagnosis and cardiovascular health assessment.

To assess long-term performance, the flexible patch was worn by human volunteers for an extended period, monitoring ECG signals over a duration of up to 40 days. Stability tests demonstrated the exceptional durability of the printed electrodes. Over the 40-day monitoring period, the device consistently captured high-quality ECG signals without significant degradation in signal amplitude or waveform integrity (Figure 4e). These results underscore the long-term electrical stability of the 20Sil-based conductive ink discussed above, addressing a key limitation in

© 2025 The Author(s). Advanced Materials Technologies published by Wiley-VCH GmbH

2365709x, 2025, 24, Downloaded from https://advanced.onlinelibrary.wiley.com/doi/10.1002/admt.202501154 by POLITECNICO DI MILANO, Wiley Online Library on [20/03/2026]. See the Terms and Conditions (https://onlinelibrary.wiley.com/terms-and-conditions) on Wiley Online Library for rules of use; OA articles are governed by the applicable Creative Commons License

conventional polymer-based electrodes. The composite approach addresses key challenges related to conductivity loss over time due to oxidation, mechanical fatigue, and material degradation. Beyond ECG monitoring, the stability and mechanical flexibility of these printed patches suggest their potential for broader bioelectronic applications. Furthermore, the demonstrated ability to fabricate wearable patches via DIW highlights the promise of conductive polymers in low-cost wearable bioelectronics.

3. Conclusion

In this work, we presented fully 3D-printable and stable conductive polymer composites engineered for long-term bioelectronic sensing. By employing a conjugated polymer and a siloxane network-former, we developed a hybrid material that simultaneously enhances electrical conductivity, mechanical flexibility, and long-term stability. The optimized formulation achieved a conductivity of 1.7 S cm^{-1}, six orders of magnitude higher than the pristine polymer, and maintained over 85% of this performance after 60 days in open air without encapsulation. Mechanically, the composite exhibited exceptional stretchability (strain at break up to 253%) while preserving tensile strength above 25 MPa. Rheological tuning enabled the formulation of printable inks with ideal flow behavior allowing for high-resolution, shape-retaining deposition using direct ink writing. These features enabled the fabrication of soft, conformal ECG electrodes capable of acquiring high-fidelity heart signals continuously for over 40 days with no signs of mechanical or electrical failure. This study highlights the potential of integrating materials design with scalable additive manufacturing to produce conformable, low-cost, and high-performance bioelectronic interfaces. Our method offers a new approach for long-term physiological monitoring and lays the groundwork for future developments in wearable health technologies. Future research will focus on evaluating cytotoxicity, irritation, and long-term dermal compatibility, particularly under daily-use conditions. In parallel, we aim to explore alternative dopants and crosslinkers to expand the applicability of our materials toward implantable and multifunctional bioelectronic systems. Consideration of large-scale manufacturing factors, such as print speed and material cost, will also be critical to support broader adoption in healthcare settings.

4. Experimental Section

Materials: ProDOT-BDT (M_n 16 kDA) was synthesized and purified following previously reported procedures.[58] Trichloro(octyl)silane, sodium chloride (NaCl), Sylgard 184, and chloroform were purchased from Sigma–Aldrich and used as received without further purification.

Sample Preparation: Polymer composites (xSil, where x represents the chlorosilane content: x = 0, 20, 40, or 60 wt.%) were prepared by first, dissolving CP and chlorosilane in chloroform, separately, at a concentration of 20 mg mL^{-1} for at least 2 h at 40 °C to ensure complete dissolution. Blends with appropriate weight ratios were then formed by mixing the CP and Sil chloroform solution and by stirring for 30 min. xSil films were processed via spin-coating at 1000 rpm for 60 s (unless otherwise specified). Before deposition, glass substrates were sequentially cleaned by sonication in deionized water (60 °C), acetone, and isopropanol, followed by drying with nitrogen. After spin-coating, samples were annealed at 70 °C for 30 min in an oven to promote the siloxane network formation and remove residual solvents. Films were stored under ambient conditions.

Morphological Studies: UV–vis absorption spectra were recorded using a PerkinElmer Lambda 1050 UV-Vis-NIR spectrophotometer. Surface morphology was examined via atomic force microscopy (AFM) using a Bruker Dimension Icon XR scanning probe microscope, with image analysis performed using Gwyddion software. Film thickness was measured using a Dektak XT profilometer.

Electrical Conductivity Measurements: Electrical conductivity of the composite films was evaluated using a Keithley 4200 analyzer in a four-point probe configuration. To assess stability under mechanical bending, the electrical conductivity of bent xSil films, deposited on Kapton tape, was measured using a two-point probe configuration under different bending radii. The initial measured values were first compared to the unbent samples to ensure accuracy, then, using moving probe tips, the films were subjected to different bending radii (onto different objects with measured curvatures), and the corresponding conductivity was recorded in real time under open air.

Electrochemical Characterization: Cyclic voltammetry (CV) measurements were performed in a conventional three-electrode setup, with xSil films coated onto indium tin oxide (ITO) substrates as the working electrode, a platinum spiral wire as the counter electrode, an Ag/AgCl reference electrode, a 0.1 M NaCl as the electrolyte, and 20 mV s^{-1} as the scan rate. The electrolyte solution was degassed with N_2 for at least 30 min prior to measurements. Electrochemical impedance spectroscopy (EIS) measurements were conducted over a frequency range of 10^{-1} to 10^6 Hz with an AC voltage amplitude of 10 mV.

Mechanical Tests: Mechanical properties were assessed via uniaxial tensile tests using a CellScale UniVert system equipped with a 250 N load cell. Thin-film double-layer PDMS/xSil dog-bone specimens (Figure S7, Supporting Information) were tested at a strain rate of 1 mm min^{-1}, 3 days after the processing. At least three specimens per composition were tested. Sylgard 184 was spin-coated onto glass substrates (2000 rpm, 60 s) and thermally cured at 120 °C for 20 min before deposition of xSil films. The composite films were then laser-cut into standard dog-bone geometries and carefully detached from the glass substrates. Stress-strain curves were analyzed to determine ultimate tensile strength and elongation at break.

Ink Formulation and 3D Printing: Inks were formulated by dissolving 20Sil at concentrations of 20 wt.% in chloroform. Rheological properties were assessed using a TA Instruments Discovery DHR2 rheometer with a Peltier plate at 25 °C and a cone-plane geometry (20 mm).

3D printing was carried out using a Corning Matribot Bioprinter. Ink's shape fidelity was quantified following established methods[59] through filament fusion and pore geometry tests, with the printability index (P_r) defined as:

$$P_r = \frac{p^2}{16A} \tag{1}$$

where p is the pore perimeter and A is the pore area.

Printing parameters of the formulated ink included a speed of 10 mm s^{-1}, an extrusion rate of 1 µL s^{-1}, a nozzle diameter of 200 µm, and a layer height of 80 µm at 23 °C. The metrology of the printed pattern was performed using optical microscopy, followed by image analysis with the open-access software ImageJ.

Patches Fabrication and Electrocardiogram Sensing: Flexible ECG patches were fabricated as illustrated in Figure S9 (Supporting Information) by first 3D printing Sylgard 184 as a substrate, followed by thermal curing at 120 °C for 20 min. The 20Sil-based ink was subsequently printed onto the cured substrate and annealed at 70 °C for 30 min. A commercial biocompatible adhesive layer (Lepu Medical) was applied to ensure skin contact (Figure S9, Supporting Information). The patch was connected via a standard plug to a PC80B electrocardiogram (ECG) monitoring system (Lepu Medical). ECG measurements were performed on human subjects while seated upright at ambient with minimal movement. The recorded signals were then exported and analyzed using a custom Python script. After every use, the patches were stored at ambient until the next measurements.

© 2025 The Author(s). Advanced Materials Technologies published by Wiley-VCH GmbH

2365709x, 2025, 24, Downloaded from https://advanced.onlinelibrary.wiley.com/doi/10.1002/admt.202501154 by POLITECNICO DI MILANO, Wiley Online Library on [20/03/2026]. See the Terms and Conditions (https://onlinelibrary.wiley.com/terms-and-conditions) on Wiley Online Library for rules of use; OA articles are governed by the applicable Creative Commons License

Statistical Analysis: Data analysis and plotting was performed using OriginLab software and plotted as mean ± SDs for a minimum of three samples measured independently or otherwise specified in the Experimental section. For the aging tests, the samples were left in the open inside the research laboratory at MIT. The ECG recordings were performed indoor while volunteers were seated with no particular restriction of their overbody movements.

Supporting Information

Supporting Information is available from the Wiley Online Library or from the author.

Acknowledgements

S.B. gratefully acknowledges financial support from the Progetto Roberto Rocca Doctoral Fellowship. The authors acknowledge MIT.nano and the MIT Materials Research Laboratory (MRL) for providing access to their facilities, where part of this work was conducted. A.G. thanks the research group of Prof. Jianguo Mei for the synthesis of the conjugated polymer. The authors also acknowledge the use of Blender for artistic illustrations.

Conflict of Interest

The authors declare no conflict of interest.

Data Availability Statement

The data that support the findings of this study are available in the supplementary material of this article.

Keywords

3D printing, conductivity, electrophysiological sensing, organic electronics, polymer composites

Received: May 30, 2025
Revised: August 14, 2025
Published online: September 7, 2025

[1] X. Gu, C. Yao, Y. Liu, *Adv. Healthcare Mater.* **2016**, *5*, 2345.
[2] Y. Xiong, L. Qi, Y. Niu, Y. Lin, Q. Xue, Y. Zhao, *Adv. Intell. Syst.* **2020**, *2*, 1900124.
[3] J. T. Santini, M. J. Cima, R. Langer, *Nature* **1999**, *397*, 335.
[4] C. Steiger, A. Abramson, P. Nadeau, A. P. Chandrakasan, R. Langer, G. Traverso, *Nat. Rev. Mater.* **2019**, *4*, 83.
[5] S. Gong, Y. Lu, J. Yin, A. Levin, W. Cheng, *Chem. Rev.* **2024**, *124*, 455.
[6] A.-M. M. Pappa, O. Parlak, G. Scheiblin, P. Mailley, A. Salleo, R. M. Owens, *Trends Biotechnol.* **2018**, *36*, 45.
[7] J. Min, J. R. Sempionatto, H. Teymourian, J. Wang, W. Gao, *Biosens. Bioelectron.* **2021**, *172*, 112750.
[8] Y. Luo, M. R. Abidian, J.-H. Ahn, D. Akinwande, A. M. Andrews, M. Antonietti, Z. Bao, M. Berggren, C. A. Berkey, C. J. Bettinger, J. Chen, P. Chen, W. Cheng, X. Cheng, S.-J. Choi, A. Chortos, C. Dagdeviren, R. H. Dauskardt, C. Di, M. D. Dickey, X. Duan, A. Facchetti, Z. Fan, Y. Fang, J. Feng, X. Feng, H. Gao, W. Gao, X. Gong, C. F. Guo, et al., *ACS Nano* **2023**, *17*, 5211.
[9] E. J. Fogt, L. M. Dodd, E. M. Jenning, A. H. Clemens, *Clin. Chem.* **1978**, *24*, 1366.
[10] Y. Luo, B. Zhu, S. Zhang, P. Zhang, X. Li, L. Wang, B. Lu, J. Travas-Sejdic, *Adv. Mater. Technol.* **2022**, *7*, 2101571.
[11] S. Templer, *Front. Endocrinol.* **2022**, *13*, 919942.
[12] M. Shichiri, Y. Yamasaki, R. Kawamori, N. Hakui, H. Abe, *Lancet* **1982**, *320*, 1129.
[13] T. Someya, Z. Bao, G. G. Malliaras, *Nature* **2016**, *540*, 379.
[14] C. Wang, X. Chen, L. Wang, M. Makihata, H.-C. Liu, T. Zhou, X. Zhao, *Science* **2022**, *377*, 517.
[15] J. Deng, H. Yuk, J. Wu, C. E. Varela, X. Chen, E. T. Roche, C. F. Guo, X. Zhao, *Nat. Mater.* **2020**, *20*, 229.
[16] H. Yuk, B. Lu, X. H B Zhao, *Chem. Soc. Rev.* **2019**, *48*, 1642.
[17] J. Deng, J. Wu, X. Chen, T. L. Sarrafian, C. E. Varela, W. Whyte, C. F. Guo, E. T. Roche, L. G. Griffiths, H. Yuk, C. S. Nabzdyk, X. Zhao, *Sci. Transl. Med.* **2024**, *16*, ado9003.
[18] A. S. Farooq, P. Zhang, *Sens. Actuators Phys.* **2022**, *344*, 113715.
[19] Y. Li, A. F. Rodríguez-Serrano, S. Y. Yeung, I.-M. Hsing, *Adv. Mater. Technol.* **2022**, *7*, 2101435.
[20] T. Zeng, Y. Wu, M. Lei, *Adv. Compos. Hybrid Mater.* **2024**, *7*, 141.
[21] M. S. Lee, A. Paul, Y. Xu, W. D. Hairston, G. Cauwenberghs, *Front. Electron.* **2022**, *2*, 700363.
[22] A. Gruetzmann, S. Hansen, J. Müller, *Physiol. Meas.* **2007**, *28*, 1375.
[23] A. C. Myers, H. Huang, Y. Zhu, *RSC Adv.* **2015**, *5*, 11627.
[24] T. R. Ray, J. Choi, A. J. Bandodkar, S. Krishnan, P. Gutruf, L. Tian, R. Ghaffari, J. A. Rogers, *Chem. Rev.* **2019**, *119*, 5461.
[25] M. Han, L. Chen, K. Aras, C. Liang, X. Chen, H. Zhao, K. Li, N. R. Faye, B. Sun, J.-H. Kim, W. Bai, Q. Yang, Y. Ma, W. Lu, E. Song, J. M. Baek, Y. Lee, C. Liu, J. B. Model, G. Yang, R. Ghaffari, Y. Huang, I. R. Efimov, J. A. Rogers, *Nat. Biomed. Eng.* **2020**, *4*, 997.
[26] D.-H. Kim, N. Lu, R. Ma, Y.-S. Kim, R.-H. Kim, S. Wang, J. Wu, S. M. Won, H. Tao, A. Islam, K. J. Yu, T. Kim, R. Chowdhury, M. Ying, L. Xu, M. Li, H.-J. Chung, H. Keum, M. McCormick, P. Liu, Y.-W. Zhang, F. G. Omenetto, Y. Huang, T. Coleman, J. A. Rogers, *Science* **2011**, *333*, 838.
[27] X. Liu, H. Yuk, S. Lin, G. A. Parada, T.-C. Tang, E. Tham, C. de la Fuente-Nunez, T. K. Lu, X. Zhao, *Adv. Mater.* **2018**, *30*, 1704821.
[28] M. Lay, M. G. Say, I. Engquist, *Adv. Mater. Technol.* **2023**, *8*, 2300652.
[29] T. Zhang, N. Liu, J. Xu, Z. Liu, Y. Zhou, Y. Yang, S. Li, Y. Huang, S. Jiang, *Innovation* **2023**, *4*, 100485.
[30] S. S. Mirbakht, A. Golparvar, M. Umar, B. A. Kuzubasoglu, F. S. Irani, M. K. Yapici, *Adv. Sci.* **2025**, *12*, 2405988.
[31] J. Li, S. Zhang, J. Zhong, B. Bao, K. Guo, Y. Zhang, K. Yang, Y. Tong, D. Qiu, H. Yang, H. Cheng, *Adv. Funct. Mater.* **2025**, *35*, 2504481.
[32] Y. Liu, M. Pharr, G. A. Salvatore, *ACS Nano* **2017**, *11*, 9614.
[33] G. Ren, J. Yang, X. Wang, G. Hu, H. Chen, Q. Fang, A. Yang, *ACS Appl. Polym. Mater.* **2025**, *7*, 5407.
[34] Y. Zhou, Z. Huang, Y. Chen, X. Dong, F. Fan, L. Chen, B. Feng, *Adv. Mater. Technol.* **2025**, *10*, 2401812.
[35] S. Middya, A. Carnicer-Lombarte, S. Sawiak, S. Hilton, V. F. Curto, D. G. Barone, G. S. K. Schierle, G. G. Malliaras, *Adv. Funct. Mater.* **2025**, *35*, 2417312.
[36] H. Yuk, B. Lu, S. Lin, K. Qu, J. Xu, J. Luo, X. Zhao, *Nat. Commun.* **2020**, *11*, 1604.
[37] M. B. Hasan, M. M. Parvez, A. Y. Abir, M. F. A Ahmad, *Heliyon* **2025**, *11*, 42375.
[38] Pooja, A. Kumar, P. Prasher, H. Mudila, *Carbon Lett.* **2023**, *33*, 307.
[39] Y. Wang, S. Wustoni, J. Surgailis, Y. Zhong, A. Koklu, S. Inal, *Nat. Rev. Mater.* **2024**, *9*, 249.
[40] S. T. M. Tan, A. Gumyusenge, T. J. Quill, G. S. LeCroy, G. E. Bonacchini, I. Denti, A. Salleo, *Adv. Mater.* **2022**, *34*, 2110406.
[41] B. D. Paulsen, K. Tybrandt, E. Stavrinidou, J. Rivnay, *Nat. Mater.* **2020**, *19*, 13.
[42] A. Gumyusenge, *Acc. Mater. Res.* **2022**, *3*, 669.

© 2025 The Author(s). Advanced Materials Technologies published by Wiley-VCH GmbH

2365709x, 2025, 24, Downloaded from https://advanced.onlinelibrary.wiley.com/doi/10.1002/admt.202501154 by POLITECNICO DI MILANO, Wiley Online Library on [20/03/2026]. See the Terms and Conditions (https://onlinelibrary.wiley.com/terms-and-conditions) on Wiley Online Library for rules of use; OA articles are governed by the applicable Creative Commons License

[43] H. Roh, S. Yue, H. Hu, K. Chen, H. J. Kulik, A. Gumyusenge, *Adv. Funct. Mater.* **2023**, *33*, 2304893.
[44] Z. Ke, L. You, D. T. Tran, J. He, K. Perera, A. Gumyusenge, J. Mei, *ACS Appl. Polym. Mater.* **2021**, *3*, 1537.
[45] X. Li, K. Perera, J. He, A. Gumyusenge, J. Mei, *J. Mater. Chem. C* **2019**, *7*, 12761.
[46] C. Y. Kao, B. Lee, L. S. Wielunski, M. Heeney, I. McCulloch, E. Garfunkel, L. C. Feldman, V. Podzorov, *Adv. Funct. Mater.* **2009**, *19*, 1906.
[47] J. Kim, H. Kweon, H. W. Park, P. Go, H. Hwang, J. Lee, S.-J. Choi, D. H. Kim, *ACS Appl. Mater. Interfaces* **2020**, *12*, 55107.
[48] J. Shin, H. W. Park, S. Kim, J. Yang, J. Kim, H. W. Park, D. H. Kim, M. S. Kang, *J. Mater. Chem. C* **2019**, *7*, 14889.
[49] J. Xu, S. Wang, G.-J. N. Wang, C. Zhu, S. Luo, L. Jin, X. Gu, S. Chen, V. R. Feig, J. W. F. To, S. Rondeau-Gagné, J. Park, B. C. Schroeder, C. Lu, J. Y. Oh, Y. Wang, Y.-H. Kim, H. Yan, R. Sinclair, D. Zhou, G. Xue, B. Murmann, C. Linder, W. Cai, J. B.-H. Tok, J. W. Chung, Z. Bao, *Science* **2017**, *355*, 59.
[50] X. Wang, K. Chen, L. S. de Vasconcelos, J. He, Y. C. Shin, J. Mei, K. Zhao, *Nat. Commun.* **2020**, *11*, 211.
[51] S. Zhang, C. Ge, R. Liu, *Sens. Actuators A: Phys.* **2022**, *341*, 113580.
[52] S. B. Balani, S. H. Ghaffar, M. Chougan, E. Pei, E. Şahin, *Results Eng.* **2021**, *11*, 100257.
[53] S. Bagatella, L. Guida, G. Scagnetti, E. Gariboldi, M. Salina, N. Galimberti, L. Castoldi, M. Cavallaro, R. Suriano, M. Levi, *Polymer* **2025**, *317*, 127899.
[54] I. B. Dimov, M. Moser, G. G. Malliaras, I. McCulloch, *Chem. Rev.* **2022**, *122*, 4356.
[55] S. Middya, A. Carnicer-Lombarte, S. Sawiak, S. Hilton, V. F. Curto, D. G. Barone, G. S. K. Schierle, G. G. Malliaras, *Adv. Funct. Mater.* **2025**, *35*, 2417312.
[56] D. Khodagholy, J. N. Gelinas, T. Thesen, W. Doyle, O. Devinsky, G. G. Malliaras, G. Buzsáki, *Nat. Neurosci.* **2015**, *18*, 310.
[57] A. A. Gharia, C. J. Bradfield, E. P. W. Jenkins, I. D. C. Fraser, G. G. Malliaras, *Sci. Adv.* **2024**, *10*, ado5042.
[58] C. M. Amb, P. M. Beaujuge, J. R. Reynolds, *Adv. Mater.* **2010**, *22*, 724.
[59] A. Schwab, R. Levato, M. D'Este, S. Piluso, D. Eglin, J. Malda, *Chem. Rev.* **2020**, *120*, 11028.

© 2025 The Author(s). Advanced Materials Technologies published by Wiley-VCH GmbH

2365709x, 2025, 24, Downloaded from https://advanced.onlinelibrary.wiley.com/doi/10.1002/admt.202501154 by POLITECNICO DI MILANO, Wiley Online Library on [20/03/2026]. See the Terms and Conditions (https://onlinelibrary.wiley.com/terms-and-conditions) on Wiley Online Library for rules of use; OA articles are governed by the applicable Creative Commons License